Proceedings of the First European Conference on Space Debris, Darmstadt, Germany, 5-7 April 1993 (ESA SD-01)

OPTICAL SENSING OF OBJECTS IN THE GEOSTATIONARY RING: IMPLICATIONS FOR DEBRIS POPULATION MODELS

R. Crowther[1], J.S.B. Dick[2], R.P. Edwin[3], and N.M. Parker[2]

1. Defence Research Agency, Farnborough, Hampshire, GU14 6TD, UK.
2. Royal Greenwich Observatory, Madingley Rd., Cambridge, CB3 0EZ, UK.
3. Dept. of Astronomy, University of St. Andrews, North Haugh, St. Andrews, KY16 9SS, UK.

ABSTRACT

The factors affecting the effectiveness of GEO debris detection sensors are discussed and models for the apparent motion of GEO debris in a sensor's field of view and the sensor signal environment are presented. Combining these models enables the minimum detectable size of debris to be determined as a function of orbital parameters and sensor configuration. This enables survey selection effects to be characterized. We present the results from a trial survey of a section of the GEO ring and comment on its inherent selection effects.

1. INTRODUCTION

The probability of collision between an operational satellite and a debris object is related to the their sizes and relative velocity, and the magnitude and spatial distribution of the debris population. In the geostationary ring (GEO), the collision risk is not well characterized because the catalogue of sub-metre objects at GEO altitudes is incomplete to an unknown degree.

For the low Earth orbit (LEO) environment small objects (~1cm) could be routinely detected by ground-based radars[1]. This is not possible for GEO because the r^{-4} law for radar received reflected power requires a factor of $\sim 10^6$ increase in transmitted power for the same size performance. However, surveys of the sub-metre debris population are possible using ground-based telescopes to detect the sunlight reflected from objects in LEO[2,3] and GEO[4,5].

A survey for sub-metre objects in GEO requires the highest performance from ground-based sensors and is subject to selection effects imposed by the motion of debris in the field of view. In this paper, we examine the instrument factors which affect detection performance and the selection effects as a function of orbit class. We have also carried out a trial GEO survey (in an area not covered by the GEODSS network) and discuss the demography obtained from it.

2. PERFORMANCE DEFINITION

We define the performance of a debris sensor system by two criteria: the search rate through orbital parameter space and the minimum size of detectable debris.

The search rate of orbital parameter space depends on the angular area of the sensor's field of view, the proportion of time during which the sensor can detect debris (*i.e.* the duty-cycle), and the time available for debris surveys.

Determining the minimum size of detectable debris is not so straightforward. During an exposure, debris will cast an image onto the detector. The signal-to-noise ratio created in a pixel which is part of the debris image depends on the irradiance from the debris and the number of pixels over which the received irradiance is spread during the exposure.

The irradiance is proportional to the debris area-albedo product (AAP) which is analogous to the radar cross-section (RCS) quoted for radar sensors.

The number of pixels in the debris image is a function of the sensor configuration (*e.g.* pixel field of view), the exposure duration, τ, and the angular rate of the image of the debris across the sensor's field of view, $d\theta/dt$. For a given observation, there is a minimum AAP which is just detectable.

The minimum detectable AAP may also be converted to a minimum detectable characteristic length ϕ_{min} for a generalized shape of unit albedo using the following approximation:

$$\phi_{min} \approx \sqrt{AAP_{min}} \qquad \text{(Eqn 1)}$$

(Any error in the geometrical foundations of this simple relationship is much less than the error in an assumed albedo.) From the above discussion, Eqn 1 may also be written as:

$$\phi_{min} = f(d\theta/dt,\ \eta) \qquad \text{(Eqn 2)}$$

where η is a measure of the sensor's ability to dis-

tinguish debris irradiance from the (noise) background - *i.e.* a function of the sensor configuration.

Thus, to determine the effectiveness of any sensor or survey in terms of the ability to detect objects of a given size in a given type of orbit, it is necessary to

- determine how $d\theta/dt$ is driven by the orbital parameters $\{a,e,i,\omega,\Omega,t_o\}$, and
- define f as a function of $d\theta/dt$ and the sensor configuration

Eqn 2 may then be expressed as a function of orbit, and sensor configuration and used to establish the effectiveness of any particular sensor in detecting debris in any given orbit:

$$\phi_{min}=f(\{a,e,i,\omega,\Omega\}, \text{sensor}) \qquad \text{(Eqn 3)}$$

3. ORBITAL KINEMATICS MODEL

The angular rate, $d\theta/dt$, as a function of $\{a,e,i,\omega,\Omega\}$ may be determined as follows. The longitude, λ, and declination, δ, of a satellite in a nominal geosynchronous orbit as observed from the geocentre are given approximately by [6,7]:

$$\lambda = \lambda_o + (n-\omega_E)t + 2e\sin(nt) - (i/2)^2 \sin(2(nt+\omega)) \qquad \text{(Eqn 4)}$$

$$\delta = i\sin(nt+\omega) \qquad \text{(Eqn 5)}$$

where we define

i	satellite orbital inclination (rads)
n	mean motion of satellite (rads s^{-1})
ω_E	Earth's angular velocity (rads s^{-1})
e	satellite orbit eccentricity
ω	satellite argument of perigee (rad)
t	elapsed time since perigee passage (s)
λ_o	satellite longitude at epoch (rad)
a	satellite orbit semi-major axis (km)
a_{GEO}	semi-major axis of GEO orbit (km)
Δa	$a-a_{GEO}$

If the observing station is not located on the equator below the satellite then correction must be made for the relative position of the station to the nodal crossing.

The influence on the observed motion of a satellite of departures from the nominal geostationary values of $\{a,e,i\}$ are illustrated in Fig 1 through Fig 3.

Each frame in those figures represents a 3° by 3° field of view. Fig 4 shows the influence of ω on the observed motion. In all test cases, the departures from GEO take the values Δa=0km, e=0.005, i=1.5°, ω=0° unless that variable is the one being varied. The time step between each of the points is one hour. It is clear that i) departure from the GEO value of semi-major axis results in a translation of the node and the eventual movement of the object out of the field of view, ii) non-zero eccentricity results in the spreading of the observed trajectory motion in a horizontal direction, iii) non-zero inclination causes motion in the vertical direction (the extent of which equals i), and iv) the value of ω will determine the shape of the observed satellite trajectory . The angular rate is obtained by differentiating Eqn 4 and Eqn 5 with respect to time, so enabling a value for $d\theta/dt$ to be found.

$$d\lambda/dt = n-\omega_E + 2en\cos(nt) - (n/2)i^2\cos(2(nt+\omega)) \qquad \text{(Eqn 6)}$$

$$d\delta/dt = ni\cos(nt+\omega) \qquad \text{(Eqn 7)}$$

$$d\theta/dt = \sqrt{((d\lambda/dt)^2+(d\delta/dt)^2)} \qquad \text{(Eqn 8)}$$

In these examples, the angular rate remains below 0.5"/s; for i~90°, $d\theta/dt$ could reach ~15"/s.

4. SIGNAL ENVIRONMENT MODEL

The determination of η requires the calculation of the signal-to-noise ratio (SNR) for a sensor system. The SNR in a pixel is a function of the irradiance from the debris and the noise in the debris and non-debris signals received by the sensor.

In order to estimate the SNR, we have developed a model of the signal environment seen by the sensor and calibrated the model's constants with observations.

We define

κ_{deb}	photons/s/nm/m^2/m^2 from GEO debris
κ_{sky}	photons/s/nm/m^2/sq" from sky
τ	exposure time (s)
$\delta\lambda$	system passband (nm)
λ	wavelength of observation (nm)
d	diameter of telescope (m)
ϕ	characteristic size of debris (m)
ε_o	optics efficiency
ε_d	detector quantum efficiency
b	atmospheric/system psf (fwhm,")
A	debris albedo
$d\theta/dt$	debris angular velocity ("/s)
p_d	pixel (detector) size in μm
p_α	pixel size in arcsec
f	focal ratio of telescope

The signal (per exposure) from the debris is:

$$s_{deb}=\kappa_{deb}\delta\lambda\varepsilon_o\varepsilon_d d^2\phi^2\tau\tau/4 \qquad \text{(Eqn 10)}$$

and from the sky (per pixel, per exposure) is:

$$s_{sky}=\kappa_{sky}\delta\lambda\varepsilon_o\varepsilon_d d^2(p_\alpha)^2\tau\tau/4 \qquad \text{(Eqn 11)}$$

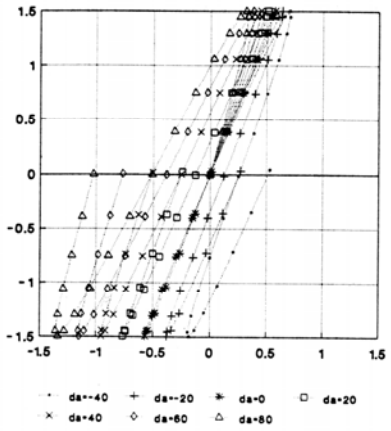

Fig 1 Effect of non-zero Δa on satellite position.

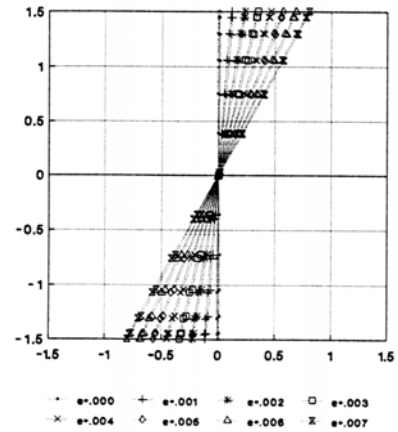

Fig 2 Effect of eccentricity on satellite position

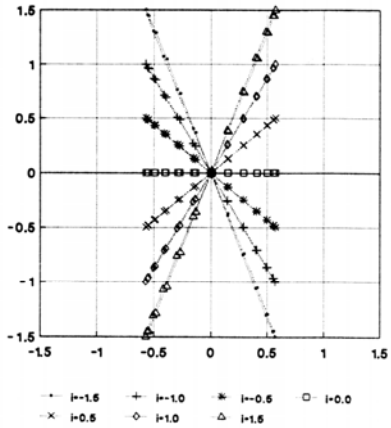

Fig 3 Effect of inclination on satellite position

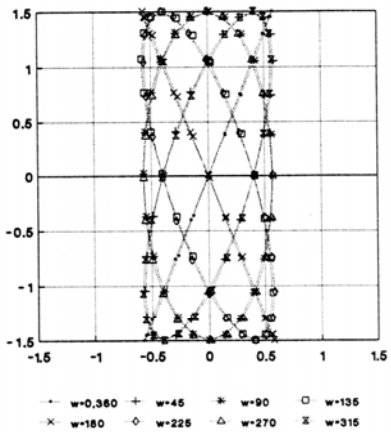

Fig 4 Effect of ω on satellite position

We ignore any detector thermal noise or read-out noise since both of these are much smaller than the noise in the sky background.

The angular motion of the debris during the exposure and the blurring ("seeing") of the Earth's atmosphere result in the signal from the debris being spread across a rectangular path, w pixels wide and l pixels long. For Nyquist sampling of the atmospheric seeing, $2p_\alpha \sim b$. However, for debris detection, we are interested only in obtaining the maximum SNR per pixel and undersampling is allowed. Hence, the minimum values for w and l are:

$$w = \max(2, b/p_\alpha) \qquad \text{(Eqn 12)}$$

$$l = \max(2, (b + \tau\, d\theta/dt)/p_\alpha) \text{ and} \qquad \text{(Eqn 13)}$$

$$N = w\, l \qquad \text{(Eqn 14)}$$

The lower limit of 2 on w and l is to cover the case when the debris image is bisected by pixel boundaries in both x and y; for large pixels ($p_\alpha >> b$) much of the image trail may have sections with unit width: our SNR estimate is thus conservative.

Combining Eqn 10, Eqn 11, and Eqn 14 gives the signal-to-noise ratio per pixel:

$$\text{SNR} = \frac{s_{deb}/N}{\sqrt{(s_{deb}/N + s_{sky})}} \qquad \text{(Eqn 15)}$$

Defining ϕ_{min} as being the size of debris to produce an SNR=1 (*i.e.* the noise equivalent diameter, NED), Eqn 15 may be solved numerically to give:

$$\phi_{min}=f(d\theta/dt,\tau,\delta\lambda,d,\varepsilon_o,\varepsilon_d,b,p_\alpha) \quad \text{(Eqn 16)}$$

for a given κ_{deb} and κ_{sky}.

Values for κ_{deb} and κ_{sky} have been obtained from theory and observation. For λ~600nm, κ_{deb}~250 for a Lambertian scatterer. (Observations of the defunct Meteosat 3 using this value of κ_{deb} imply an albedo of ~0.1.)

κ_{sky}~0.1 for a dark, high altitude site and ~2.5 for a low-altitude site with some contamination from artificial lighting.

5. SENSOR PERFORMANCE

Inspection of Eqn 15 shows that ϕ_{min} may be minimized by maximizing any of $\delta\lambda$, d, ε_o, ε_d and minimizing κ_{sky}. ε_d may be optimized by choosing a detector whose quantum efficiency, QE(λ), is matched to the solar irradiance I(λ) - a condition easily met by CCDs: state-of-the-art thin CCDs achieve ε_d~80+%.

The optimal choice of τ and p_α for a given sensor configuration (*i.e.* b and p_α) and orbit type (which determines $d\theta/dt$) is not determinable by inspection. However, using results from numerical modeling, it is clear that ϕ_{min} is strongly influenced by the orbit type and exposure duration, as shown in Fig 5.

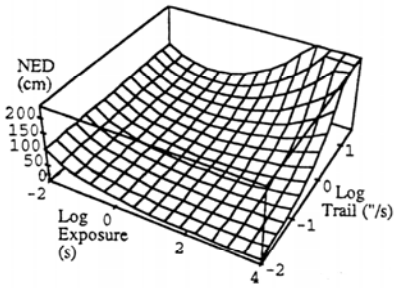

Fig 5 ϕmin as a function of $d\theta/dt$ and τ

The sensor pixel size may also be optimized. For $d\theta/dt$~0, *N* is a function of the *ratio* of b/p, not an absolute value of p, although there may be a better smaller p for situations where κ_{sky} is large. For t $d\theta/dt$>>b, a substantial trail may be visible and *N* will be minimized for (b/p) <0.5 with the exact value dependent on κ_{sky}.

The practical limit to the pixel size is a trade-off between optimising the SNR in each pixel and the usefulness of a trail for determination of motion vector.

Optimal pixel sizes usually demand unrealisable optical systems focal ratios but may be synthesised by on-chip binning of CCD pixels.

6. SURVEY

We have undertaken a limited survey of the GEO region 0.1°E to 5.75°W and from 0.2°S to 0.2°N. using the James Gregory Telescope at the University Observatory, St Andrews (2° 48.9'W,+56° 20.2'N). The telescope, which was originally used for wide-field (4°) photography, is of the Cassegrain-Schmidt type and was designed by Linfoot[8] who pioneered this now popular optical configuration. However, modern examples are all of small aperture and the St Andrews instrument is believed to be the largest of its type. The full aperture of the telescope is 0.95m and the effective focal length of 2.58m produces an image scale of 80 arcseconds per millimeter on a flat focal plane, ideal for CCD detectors.

In 1992 a cooled CCD camera was acquired for the telescope with funds from the UK Science and Engineering Research Council. The camera, manufactured by Wright Instruments, London, incorporates an EEV type 02-06 front illuminated CCD and is of the MPP (multi-pinned phase) type which achieves a very low thermal background of 10^{-3} electrons/pixel/second at temperatures of ~200K, maintained by a four stage Peltier cooler. The readout noise is 5.8 electrons RMS and the pixel signals are digitized to 16 bits at a gain setting of 5 electrons per ADU. Pixel saturation occurs at 1.5×10^5 electrons approximately. The full frame area of the CCD element contains 385x578 22μm (square) pixels and records 12'x17' of sky.

At each survey position, two frames were taken in the R band (λ_o~650nm, $\delta\lambda$~150nm). The exposure time was chosen to optimize the detection of small objects with low drift rates; each frame was exposed for 90s with an inter-frame gap of 60s. This double-exposure technique discriminates against random events affecting only one frame, such as cosmic ray hits, and also gives some indication of object angular rate and direction of travel. The observations were taken at dark of Moon and when the GEO co-ordinates were sunlit.

The noise floor in each frame is dominated by the Poisson noise in the sky signal. Frames were processed to remove pixel-to-pixel sensitivity variations prior to analysis for debris detection.

The computed value of ϕ_{min} (as a function of $d\theta/dt$) for this survey is shown inFig 6.

The survey found no objects which are not identifiable from the ESA GEO catalog[9].

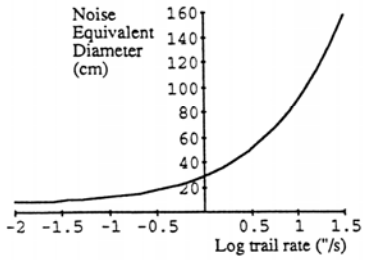

Fig 6 ϕ_{min} as a function of $d\theta/dt$ for this survey

7. COMMENTARY

Upper limits on the GEO population in the area surveyed may be estimated by assuming debris to be randomly distributed throughout a band 360° long by 20° wide. Such a surface area could be surveyed using about $2x10^5$ frames equal in area to our survey's CCD frames.

We assume the population is sparsely distributed and so Poissonian probability techniques may be applied[10]. If the total population is p then the probability per field is $p/2x10^5$. For ~60 sample fields (s=60) the mean value, μ, expected is $sp/2x10^5$. The probability of k detections is

$$P(k)=\mu^k e^{-\mu}/k! \qquad \text{(Eqn 17)}$$

For a 50% probability of zero detections,

$$\mu=-\log_e(0.5)=sp/2x10^5 \qquad \text{(Eqn 18)}$$

which implies that our null detection would have a 50% probability with $p\sim2x10^3$ debris particles with $\phi>\phi_{min}$ in GEO; the probability of zero detections is only 1% with a population size of $\sim2x10^4$.

However, from our discussion of sensor sensitivity as a function of debris apparent angular speed, we know that our survey has only been sensitive to objects larger than 10cm with unit albedo (or ~60cm for albedo=0.03) *and* with small drift rates characteristic of orbits with near-zero e, i, and Δa. For orbits with high inclinations, ϕ_{min}>80cm: our survey has *not* sampled these orbits for sub-metre debris.

It is clear that surveys of longer duration are required to establish accurate estimates of the GEO population and that sensors must be deployed in a number of configurations in order to detect small debris in orbits with high inclination and/or high eccentricity as might result from satellite break up events. Our modeling of optical sensing of objects in the GEO ring gives us a good understanding of the performance of sensor systems and of the selection effects encountered during surveys - and such selection efects have important implications for debris population models derived from surveys.

The original research for this project was carried out under a contract from ESA, with Sira Ltd, Chislehurst, UK, as prime contractor; later research was funded by BNSC under grant ROAME ATS 7/1. JSBD would like to thank Drs Andrew Sinclair and Graham Appleby for useful conversations and supplying images of Meteosat-3.

8. REFERENCES

[1] Beusch, J., Kupiec, I., "NASA debris environment characterization with the Haystack radar" *AIAA/NASA/DoD Orbital debris conference, Baltimore,* April 16-19, 1990.

[2] Henize, K., Stanley, J. "Optical observations of space debris" *AIAA/NASA/DoD Orbital debris conference, Baltimore,* April 16-19, 1990.

[3] Henize, K.G., O'Neill, C.A., Mulrooney, M.K.,*AIAA/NASA/DoD Orbital debris conference, Baltimore,* April 16-19, 1990.

[4] Gehrels, T., Vilas, F. A CCD search for geosynchronous debris. *Icarus* **68**, 412, 1986.

[5] Boehnhardt, H. Photographic observations of the co-located spacecraft at 19° West, *Technical Report*, c/o ESOC, Darmstadt.

[6] Merson, R.H., Satellite orbit and attitude theory and its use with Skynet 2, *RAE Technical Report 77083*, June 1977.

[7] Fitzpatrick, P.M., in *Principles of Celestial Mechanics*, Academic Press, 1970.

[8] Linfoot E.H. *Proc. phys. Soc.* 58-65-1946.

[9] Janin, G., A log of objects near the geostationary ring, *Mission analysis section, European Space Operations Centre, Darmstadt*.

[10] Rényi, A., in *Probability Theory*, Publishing house of the Hungarian Academy of Sciences, Budapest, 1970.